

# Evolution of $\beta$ -decay half-lives at finite-temperatures

A. Ravlić,<sup>1,\*</sup> E. Yüksel,<sup>2,†</sup> Y.F. Niu,<sup>3</sup> and N. Paar<sup>1,‡</sup>

<sup>1</sup>*Department of Physics, Faculty of Science, University of Zagreb, Bijenička c. 32, 10000 Zagreb, Croatia*

<sup>2</sup>*Physics Department, Faculty of Arts and Science, Yildiz Technical University, Istanbul, Turkey*

<sup>3</sup>*School of Nuclear Science and Technology, Lanzhou University, Lanzhou, China*

(Dated: July 7, 2022; Revised August 2020)

$\beta$ -decay half-lives of nuclei at finite temperature are investigated in the framework of relativistic nuclear energy density functional. Both thermal and nuclear pairing effects are included in the description of nuclear ground-state properties and in the finite temperature proton-neutron relativistic quasiparticle random-phase approximation (FT-PNRQRPA) to account for the relevant allowed and first-forbidden transitions in the  $\beta$ -decay. The temperature effects are studied in detail on the  $\beta$ -decay half-lives and related GT<sup>-</sup> transitions in Ar, Fe, Cd, and Sn isotopic chains. It is shown that in nuclei with longer half-lives the temperature effects decrease the half-lives considerably, whereas for nuclei with short half-lives only small changes are obtained. The analysis shows that the temperature can either increase or decrease the half-lives in open-shell nuclei, depending on the interplay with particular shell structure and the pairing effects. In addition, large-scale calculations of  $\beta$ -decay half-lives are performed at  $T_9(K) = 5$  and  $T_9(K) = 10$  for nuclei in the range  $8 \leq Z \leq 82$ , relevant for astrophysical nucleosynthesis mechanisms.

Nuclear  $\beta$ -decay is the fundamental property of atomic nuclei, which plays a decisive role in nuclear astrophysics [1–3] and particle physics [4–6] as well as for the properties and structure of nuclei. Within the context of nuclear astrophysics, recent studies are mainly focused on the understanding of the synthesis of elements heavier than iron via the rapid-neutron capture process ( $r$ -process) [7–10]. Along with other nuclear properties (masses, separation energies, etc.),  $\beta$ -decay half-lives are one of the most essential ingredients of the  $r$ -process calculations, determining the timescale of the process and the relative abundances of the nuclear species [1, 2]. It is also known that uncertainties in  $\beta$ -decay rates can produce significant alterations in the abundance distribution of nuclei [3]. Therefore, accurate calculations of  $\beta$ -decay properties are of utmost importance for  $r$ -process simulations. Since it is still not possible to reach experimental data for the  $\beta$ -decay half-lives of all relevant  $r$ -process nuclei, the simulations mainly rely on the theoretical predictions. We note that  $\beta$  decays in nuclear astrophysics often occur in various hot stellar environments, thus they have to be described by considering finite temperature effects. At present, theoretical description is decisive to provide nuclear properties and processes at finite temperature, necessary for astrophysical modeling.

The first tabulation of weak interaction rates for stellar environments was done by Fuller, Fowler, Newmann (FFN) [11–14]. Using the independent particle model, rate tables were created for a broad range of temperatures and stellar densities. The shell-model (SM) calculations were also performed to study  $\beta$ -decay rates of the  $sd$ -shell nuclei [15], and then extended to the  $pf$ -shell nuclei [16]. Although significant progress has

been accomplished over the years, the calculations for heavy nuclei are still demanding due to the huge configuration space of the SM calculations [17–19]. Large-scale calculations were also performed with the quasi-particle random phase approximation (QRPA) on top of the Finite Range Droplet Model (FRDM) [20], which are mostly used in  $r$ -process simulations today. Apart from the microscopic-macroscopic models, self-consistent models based on the non-relativistic and relativistic energy density functionals were also applied to study  $\beta$ -decay properties of nuclei [21–23] and their impact on  $r$ -process calculations [24, 25]. Recently, the relativistic Hartree-Bogoliubov model (RHB) plus relativistic QRPA with momentum-dependent meson-nucleon couplings were used to calculate  $\beta$ -decay half-lives of neutron-rich nuclei in the  $Z \approx 28$  and  $Z \approx 50$  regions [26]. Using a relativistic model with momentum-dependent self-energies in the calculations, predictions for the  $\beta$ -decay rates were improved. Later on, in Ref. [27], the same model was employed to perform large-scale calculation of  $\beta$ -decay half-lives and  $\beta$ -delayed neutron emission probabilities of 5409 neutron-rich nuclei in the range  $8 \leq Z \leq 124$ , including both the allowed (GT) and first-forbidden (FF) transitions. In recent years,  $\beta$ -decay half-lives of nuclei were also studied using the (quasi)particle-vibration coupling techniques to take into account more complex configurations and obtain a better agreement with the experimental data [28–34].

Although its astrophysical site is not clear yet, the  $r$ -process is known to take place at high temperatures (1-10 GK) and neutron densities ( $n_n > 10^{20}$  g cm<sup>-3</sup>). However, temperature effects on  $\beta$ -decay rates have been scarcely explored up to now. In Ref. [35] the finite-temperature QRPA (FT-QRPA) was applied on top of the finite-temperature Skyrme-HF + Bardeen-Cooper-Schrieffer (BCS) theory in order to determine  $\beta$ -decay half-lives of  $N = 82$  isotones. It was shown that temperature effect first leads to a decrease in the  $\beta$ -decay

\* aravlic@phy.hr

† eyuksel@yildiz.edu.tr

‡ npaar@phy.hr

half-lives, whereas they also obtained an increase in the half-lives of some open-shell nuclei after  $T > 0.6$  MeV. However, Ref. [35] includes only Gamow-Teller (GT) excitations in the calculation of the total decay rate. Recently, temperature effects were studied within the finite-temperature relativistic time-blocking approximation, including single nucleon-phonon couplings [34]. It was shown that the  $\beta$ -decay rates are quite sensitive to the changes in temperature due to its impact on the low-energy region of the spin-isospin excitations.

In this Letter, we present the first study of the evolution of  $\beta$ -decay half-lives at finite temperature, including large-scale calculation for even-even nuclei, based on the self-consistent finite temperature proton-neutron relativistic QRPA. Both allowed and first-forbidden transitions are included in description of the  $\beta$ -decay half-lives at zero and finite temperatures. We choose Ar, Fe, Cd and Sn nuclei to demonstrate the different effects of temperature on the spin-isospin excitations and  $\beta$ -decay half-lives of open and closed-shell nuclei. Our work provides the first theoretical framework capable for microscopic description of temperature-dependent  $\beta$ -decay rates across the nuclide chart.

We establish the theory framework for description of  $\beta$ -decay based on the relativistic nuclear energy density functional (RNEDF) with momentum-dependent self-energies [36]. The nucleons are treated as point-particles that exchange isoscalar-scalar  $\sigma$ -meson, isoscalar-vector  $\omega$ -meson and isovector-vector  $\rho$ -meson (see Refs. [37, 38]). In contrast to usual RNEDFs, additional couplings between nucleon and meson fields are present, containing momentum-dependent terms, thus producing momentum-dependent self-energies. Derivative-coupling (DC) models are known to provide a higher value of the effective nucleon mass  $m^*$ , giving a higher density of the states around the Fermi level, while still having a good agreement with nuclear-matter and finite-nuclei properties [26]. In our work, we use the D3C\* parametrization from Ref. [26], which is known to produce a good agreement with experimental values of  $\beta$ -decay half-lives in medium and heavy nuclei.

In order to calculate the nuclear ground state, finite-temperature Hartree-BCS theory (FT-HBCS) is used, that includes both pairing correlations and finite-temperature effects [39, 40]. Spherical symmetry is assumed. In this work, only isovector pairing ( $T=1, S=0$ ) contributes to the ground-state calculations and leads to the partial occupation of states. The isovector pairing strength parameters  $G_{n(p)}$  are adjusted according to the five-point mass formula for each nucleus [41].

The charge-exchange excitations are calculated using the finite-temperature proton-neutron relativistic quasi-particle random-phase approximation (FT-PNRQRPA) [42–44]. Both isovector ( $T = 1, S = 0$ ) and isoscalar pairing ( $T = 0, S = 1$ ) contribute in the particle-particle ( $pp$ ) residual interaction part of the FT-PNRQRPA [45, 46]. For the isoscalar pairing, we employ formulation with a short-range repulsive Gaussian combined with a weaker

longer-range attractive Gaussian

$$V_{12} = V_0^{is} \sum_{j=1}^2 g_j e^{-r_{12}^2/\mu_j^2} \prod_{S=1, T=0} , \quad (1)$$

where  $\prod_{S=1, T=0}$  denotes projector on  $T = 0, S = 1$  states.

For the ranges we use  $\mu_1 = 1.2$  fm, and  $\mu_2 = 0.7$  fm, and strengths are set to  $g_1 = 1$  and  $g_2 = -2$  [46]. For the isovector pairing in residual interaction we employ pairing part of the Gogny interaction [47]. Isoscalar pairing strength  $V_0^{is}$  is considered as a free parameter that can be constrained by the Gamow-Teller excitation or  $\beta$ -decay experimental data. In this work, the functional form introduced in Ref. [25] is used,

$$V_0^{is} = V_L + \frac{V_D}{1 + e^{a+b(N-Z)}}, \quad (2)$$

with values  $V_L = 153.2$  MeV,  $V_D = 8.4$  MeV,  $a = 6.0$ , and  $b = -0.8$ , adjusted to best reproduce all experimentally available half-life data in the range  $8 \leq Z \leq 82$ . In the particle-hole channel ( $ph$ ) of the PNRQRPA residual interaction only  $\rho$ -meson and  $\pi$ -meson terms are present [46]. Due to the derivative nature of pion-nucleon coupling, the zero-range Landau-Migdal term is also included, that accounts for the contact part of the nucleon-nucleon interaction (see Ref. [46]). Unless otherwise stated, the strength parameter of the Landau-Migdal term is taken as  $g' = 0.76$ , which is adjusted to reproduce the experimental excitation energy of the Gamow-Teller resonance in  $^{208}\text{Pb}$ .

For the calculation of the  $\beta$ -decay half-lives both allowed ( $L = 0$ ) and first-forbidden ( $L = 0, 1$ ) transitions are included. General form of  $\beta$ -decay rate is given by

$$\lambda = \frac{\ln 2}{K} \int_0^{p_0} p_e^2 (W_0 - W)^2 F(Z, W) C(W) dp_e, \quad (3)$$

where  $W$  is electron energy in the units of  $m_e c^2$ ,  $m_e$  denotes the electron mass, and  $p_e$  is electron momentum in units of  $m_e c$ .  $W_0$  is the maximum electron energy given by difference of initial and final nuclear mass. The integration is performed up to a maximum electron momentum  $p_0$ .  $F(Z, W)$  is the Fermi function, taking into account distortion of electron wavefunctions [48]. Maximum electron energy in  $\beta$ -decay can be approximated as

$$W_0 \approx \lambda_n - \lambda_p + \Delta_{np} - E_{QRPA}, \quad (4)$$

where  $\lambda_{n(p)}$  denotes neutron(proton) chemical potentials,  $\Delta_{np} = 1.293$  MeV is the neutron-proton mass difference, and  $E_{QRPA}$  is the FT-PNRQRPA eigenvalue for the considered state.  $K$  is measured in superallowed  $\beta$ -decay to be  $K = 6144 \pm 2$  s [49].  $C(W)$  is the so-called shape factor. For the allowed GT transitions,  $C(W)$  is equal to the reduced matrix element of the  $\text{GT}^-$  transition

$$B(\text{GT}^-) = g_A^2 \frac{\langle f \parallel \sigma \tau_- \parallel i \rangle^2}{(2J_i + 1)}, \quad (5)$$

where  $\sigma$  is the Pauli spin matrix, and  $\tau_-$  is lowering isospin operator, while  $J_i$  is angular momentum of the initial state. Axial-vector coupling constant  $g_A$  is quenched from free-nucleon value of  $g_A = -1.26$  to  $g_A = -1.0$  [27, 50]. Shape factor for the first-forbidden transitions has functional form

$$C(W) = k + kaW + kb/W + kcW^2. \quad (6)$$

The details for the definitions of  $k$ ,  $ka$ ,  $kb$ ,  $kc$  can be found in Refs.[27, 51]. Finally,  $\beta$ -decay rate  $\lambda$  is connected to half-lives  $T_{1/2}$  via  $T_{1/2} = \ln(2)/\lambda$ .

As a benchmark for our study, we investigate the  $\beta$ -decay half-lives in the zero-temperature limit for Ar, Fe, Cd, and Sn isotopes, using D3C\* interaction with the Landau-Migdal term strength parameter  $g' = 0.76$  and the isoscalar pairing strength  $V_0^{is}$  as given in Eq. (2). The results shown in Fig. 1 appear in good agreement with the experimental data [52, 53]. In the case of Sn isotopes, additional improvement of the half-lives can be obtained by further adjustment of the  $g'$  value, as shown in Fig. 1(d). It is a known issue that the (Q)RPA consisting of particle-hole ( $1p-1h$ ) configuration may overestimate the half-lives of the doubly-magic nuclei [24, 27]. To improve description of the half-lives, contributions due to complex configurations should be taken into account, resulting in lower predictions of half-life by increasing the number of transitions in the low-energy region [32–34, 54]. To compensate for the shortcomings of our model for the Sn chain, we induce more strength in the low-energy region by adjusting the strength parameter of the Landau-Migdal term  $g'$  to the main GT<sup>-</sup> peak of  $^{132}\text{Sn}$ , and the best fit is obtained for  $g' = 0.5$ , as shown in Fig. 1(d). The model with the D3C\* functional benchmarked in this way at  $T = 0$  MeV, is employed in further studies of the finite temperature effects on  $\beta$ -decay.

In the upper panels of Fig. 2, we display the  $\beta$ -decay half-lives of the selected isotopic chains using the FT-PNRQRPA with D3C\* functional for the range of temperatures  $T = 0 - 1.5$  MeV. It is shown that the temperature has a considerable impact on nuclei with long  $\beta$ -decay half-lives, whereas its effect is less in short-lived nuclei. For Ar, Cd, and Sn isotopes, the half-lives almost do not change up to  $T \sim 0.3$  MeV, above which they start to decrease gradually and converge to an almost constant value at higher temperatures. As mentioned above, the influence of temperature is more pronounced for nuclei with long half-lives at zero-temperature, e.g.,  $^{44,46}\text{Ar}$ ,  $^{120}\text{Cd}$ , and  $^{130,132}\text{Sn}$ . In contrast to this behavior, the half-lives of Fe isotopes are almost independent of temperature up to the critical temperatures ( $T_c^n \sim 0.8$  MeV), and then we obtain a slight increase at higher temperatures. This increase is more pronounced for  $^{64}\text{Fe}$ , which has the longest half-life in the calculated chain.

As shown in Fig. 2, the FT-PNRQRPA half-lives for  $^{132}\text{Sn}$  are also in good agreement with the FT-RTBA results from Ref. [34]. While our calculation predicts first significant temperature effect at  $T \sim 0.3$  MeV, the FT-RTBA predicts visible effects starting from  $T \sim 0.5$

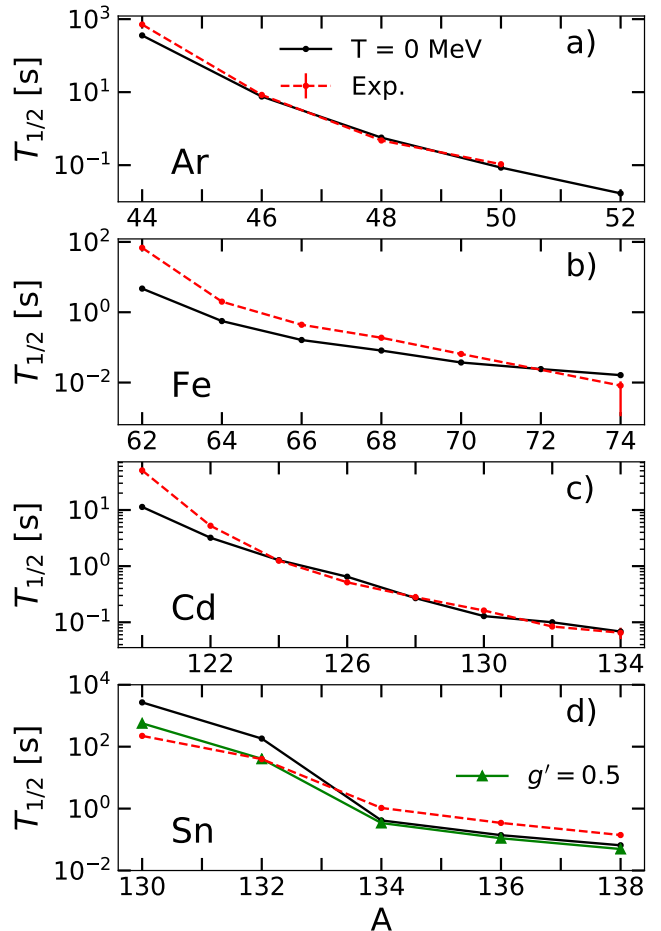


FIG. 1. Comparison between  $\beta$ -decay half-lives calculated using the FT-PNRQRPA with the D3C\* interaction using  $g' = 0.76$  (black full line) and the experimental data from Ref. [52, 53] (red dashed line) for Ar, Fe, Cd and Sn isotopic chains.

MeV. It should also be noted that both models use different effective nuclear interactions, which in turn results in different predictions for the single-particle energies and transitions relevant for the  $\beta$ -decay. At  $T = 1$  MeV, the results of both approaches agree reasonably well, and the evolution of the half-life is similar. Even though one drawback of our model is the inclusion of only two quasi-particle (q.p.) configurations within the R(Q)RPA, it includes both the pairing and temperature effects and can be applied to calculations throughout the nuclide chart, allowing large-scale calculations of relevance for astrophysical models of stellar evolution and synthesis of chemical elements.

In addition to GT<sup>-</sup> states, the first-forbidden transitions are also known to play a crucial role in the determination of the  $\beta$ -decay half-lives in certain regions of the nuclear chart [27]. Therefore, in the present analysis both allowed and first-forbidden transitions are taken into account for a proper description of the half-lives at finite temperatures. In the lower panels of Fig. 2, we dis-

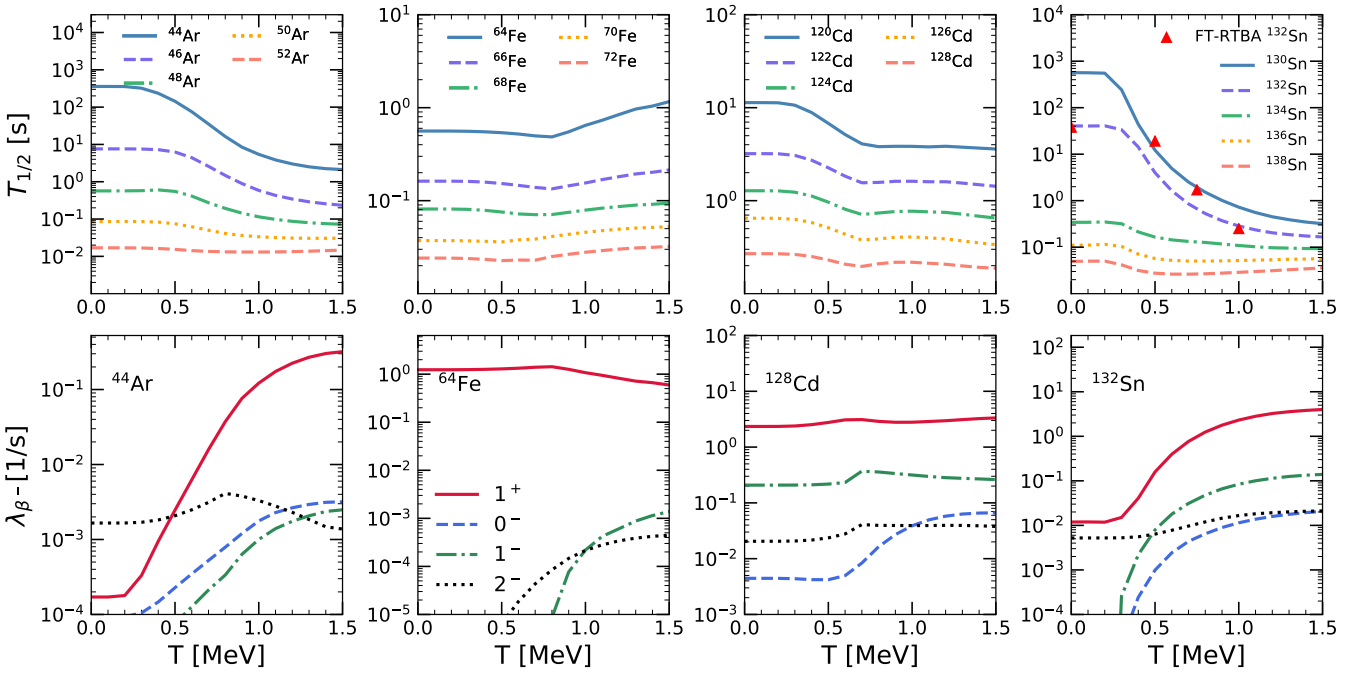


FIG. 2. Upper panels:  $\beta$ -decay half-lives  $T_{1/2}$  for Ar, Fe, Cd and Sn isotopes as a function of temperature. The calculations are performed using the FT-PNRQRPA and the D3C\* functional. Red triangles denote results of the FT-RTBA calculation for  $^{132}\text{Sn}$  from Ref. [34]. Lower panels: Temperature dependence of  $\beta$ -decay rates  $\lambda_\beta$  for both allowed ( $1^+$ ) and first-forbidden transitions ( $0^-, 1^-, 2^-$ ) for  $^{44}\text{Ar}$ ,  $^{64}\text{Fe}$ ,  $^{128}\text{Cd}$  and  $^{132}\text{Sn}$ . The  $\beta$ -decay half-lives and rates are connected to each other via  $T_{1/2} = \ln(2)/\lambda$ . See text for details.

play temperature evolution of both GT ( $1^+$  transition) and first-forbidden  $\beta$ -decay rates for  $^{44}\text{Ar}$ ,  $^{64}\text{Fe}$ ,  $^{128}\text{Cd}$  and  $^{132}\text{Sn}$ .

It is shown that for  $^{44}\text{Ar}$ , the first-forbidden multipole  $2^-$  has a larger contribution than allowed  $1^+$  up to  $T \sim 0.5$  MeV, above which  $1^+$  dominates over all other transitions due to temperature unblocking of GT $^-$  strength, as will be discussed later. Contributions of other forbidden  $0^-$  and  $1^-$  transitions also increase with temperature, but overall their impact is negligible. Good agreement with the experimental data for  $^{44}\text{Ar}$ , as shown in Fig. 1, is due to inclusion of  $2^-$  multipole, which exemplifies importance of including forbidden transitions.

On the other hand, the  $\beta$ -decay rates of  $^{64}\text{Fe}$ ,  $^{128}\text{Cd}$  and  $^{132}\text{Sn}$  nuclei are mainly determined by  $1^+$  multipole at all temperatures. For the neutron-rich and heavy  $^{128}\text{Cd}$  and  $^{132}\text{Sn}$  nuclei, other forbidden transitions also start to contribute to the  $\beta$ -decay rates, especially at higher temperatures. For instance, at low temperatures ( $T < 0.3$  MeV), both GT $^-$  and  $2^-$  transitions are important for the  $\beta$ -decay rate in  $^{132}\text{Sn}$ . By increasing temperature further,  $1^-$  and  $0^-$  transitions also have non-negligible contribution to the total  $\beta$ -decay rate above  $T > 0.3$  MeV and  $T > 0.5$  MeV, respectively. The reasons for observed changes in the  $\beta$ -decay half-lives and rates of nuclei at finite-temperature are related to temperature effects on the quasi(single)-particle properties of nuclei as well as the weakening of the residual inter-

action with increasing temperature, which in turn leads to the changes in the spin-isospin transitions in nuclei as we discuss below.

In order to analyze  $\beta$ -decay half-lives in more detail, we study the temperature effects on the GT $^-$  excitations. In Fig. 3 the calculated GT $^-$  response is shown for  $^{44}\text{Ar}$ ,  $^{64}\text{Fe}$ ,  $^{120}\text{Cd}$  and  $^{132}\text{Sn}$  at temperatures  $T = 0 - 1.5$  MeV. Enlarged insets in Fig. 3 display temperature evolution of GT $^-$  strength in the  $Q_\beta$  window, i.e. the excited states that contribute to  $\beta$ -decay half-life calculation. By increasing temperature, the main GT $^-$  peaks and the low-energy states start to slightly shift downward. However, the low-energy states within the  $Q_\beta$  window are affected differently in each nucleus with increasing temperature. Since these states are used in the calculation of the half-lives of nuclei, temperature effects in this region need to be clarified in more details to explain the results found in Fig. 2.

We start our analysis with  $^{44}\text{Ar}$  in Fig. 3(a). At  $T = 0$  MeV, the main low-energy peak is located at  $E = -0.68$  MeV with a quite low strength  $B(\text{GT}^-) = 0.04$ , which would overestimate the half-life without the contribution from  $2^-$  multipole transitions. Most of the GT $^-$  strength comes from  $\nu 1f_{7/2} \rightarrow \pi 1f_{7/2}$  transition (hereafter  $\nu$ - $\pi$  refers neutron-proton), being reduced by coherent contribution of  $\nu 1d_{3/2} \rightarrow \pi 1d_{3/2}$  and  $\nu 2s_{1/2} \rightarrow \pi 2s_{1/2}$  having the GT $^-$  matrix element with opposite sign. Up to  $T = 0.5$  MeV, the temperature does not have a big im-

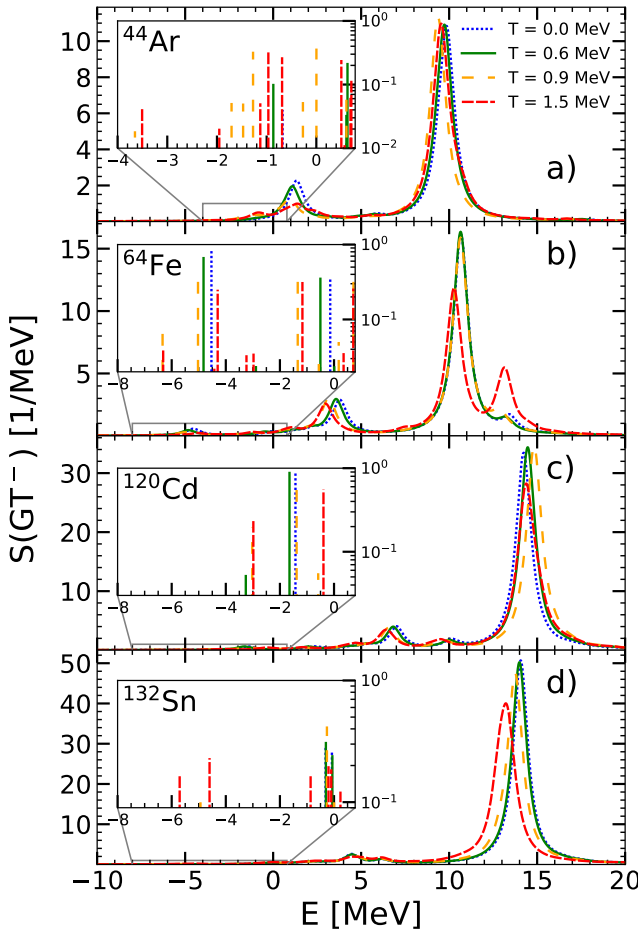


FIG. 3. The GT<sup>-</sup> strength of <sup>44</sup>Ar, <sup>64</sup>Fe, <sup>120</sup>Cd and <sup>132</sup>Sn between  $T = 0 - 1.5$  MeV. Calculations are performed with the FT-PNRQRPA based on the D3C\* interaction. Excited states are presented with respect to parent nucleus, and smeared with a Lorentzian of 1 MeV width for presentation. The insets show the excited states within the  $Q_\beta$  energy window.

pact on the nuclear ground-state properties and residual interaction of nuclei. Therefore, GT<sup>-</sup> strength almost does not change. By increasing temperature further, it is seen that the excited states start to shift downwards due to the weakening of the pairing effects and residual interaction, and new low-energy states emerge as result of the thermal unblocking. Therefore, the  $\beta$ -decay phase space increases and the lifetime decreases. For instance, at  $T = 0.6$  MeV, we obtain two main peaks at  $E = -0.87$  MeV with  $B(GT^-) = 0.10$  and  $E = 0.63$  MeV with  $B(GT^-) = 0.21$ . While the first excited state is formed with the  $\nu 1f_{7/2} \rightarrow \pi 1f_{7/2}$  transition, the second one is formed with the coherent sum of  $\nu 1d_{3/2} \rightarrow \pi 1d_{3/2}$  and  $\nu 2s_{1/2} \rightarrow \pi 2s_{1/2}$  transitions. At  $T = 0.9$  MeV pairing correlations disappear for both proton and neutron states. This sharp transition occurs due to the grand-canonical treatment of nuclei within our work [39]. Therefore, the excited states continue

to move downward, new excited states start to appear in the low-energy region due to the unblocking effect of the temperature, and the strength continues to increase within the  $Q_\beta$  window. Two main peaks are located at  $E = -1.27$  MeV with  $B(GT^-) = 0.33$  and  $E = 0.002$  MeV with  $B(GT^-) = 0.37$ , both having main contribution from  $\nu 1f_{7/2} \rightarrow \pi 1f_{7/2}$  transition. At higher temperatures, the half-lives continue to decrease smoothly, depending on the impact of the temperature on the low-energy states of the considered nuclei.

In order to better demonstrate the influence of above mentioned transitions on the half-lives, in Fig. 4 we show the temperature dependence of cumulative GT<sup>-</sup> strength in  $Q_\beta$  window (upper panels) together with the cumulative sum of half-lives  $T_{1/2}(E)$  (lower panels) calculated by restricting the phase-space integral in Eq. (3) to a limited energy window and including only GT<sup>-</sup> strength. By examining Fig. 4(a) we conclude that shifting of excitation strength to lower energies at finite-temperature leads to a significant reduction of the half-lives. At  $T = 1.5$  MeV the peak at  $E = -7.98$  MeV with relatively low strength  $B(GT^-) = 0.01$  resulting from  $\nu 1f_{5/2} \rightarrow \pi 1f_{7/2}$  transition has a huge effect on lowering the half-life. Following Eq. (3), it can be inferred that the low-energy excitations in  $Q_\beta$  window lead to a large phase-space factor, and impact the half-lives considerably.

Temperature dependence of GT<sup>-</sup> strength for <sup>64</sup>Fe is shown in Fig. 3(b) and displays a different behavior compared to <sup>44</sup>Ar. At  $T = 0$  MeV, the highest excitation peak within the  $Q_\beta$  window is located at  $E = -4.53$  MeV with  $B(GT^-) = 0.85$ . The main contribution for this state comes from the  $\nu 1f_{5/2} \rightarrow \pi 1f_{7/2}$  transition. Second highest peak is located at  $E = -0.14$  MeV with  $B(GT^-) = 0.35$ , and formed with the  $\nu 2p_{1/2} \rightarrow \pi 2p_{3/2}$  transition, together with  $\nu 2p_{3/2} \rightarrow \pi 2p_{3/2}$  transition which comes with the opposite sign in the GT<sup>-</sup> matrix element and reduces the total strength. By increasing the temperature to  $T = 0.6$  MeV, pairing effects are weakened and the excited states start to shift downwards within the  $Q_\beta$  window. The highest peak resulting from the same  $\nu 1f_{5/2} \rightarrow \pi 1f_{7/2}$  transition is now shifted to lower excitation energies and found at  $E = -4.82$  MeV while its strength is decreased to  $B(GT^-) = 0.66$ . Second peak is obtained at  $E = -0.50$  MeV with  $B(GT^-) = 0.35$ , namely, its strength remains unchanged while being shifted to lower excitation energies. Although total GT<sup>-</sup> strength is slightly reduced with increasing temperature, half-lives almost do not change due to the increase in the  $\beta$ -decay phase-space as can be inferred from Fig. 4(b). From Fig. 2 minimum of half-life is reached at  $T \sim 0.8$  MeV corresponding to the neutron(proton) pairing collapse temperature  $T_c^{n(p)}$ . By increasing temperature further, half-life starts to increase with temperature because of reduced low-lying strength in  $Q_\beta$  window, due to temperature effects on  $\nu 1f_{5/2} \rightarrow \pi 1f_{7/2}$  and  $\nu 2p_{1/2} \rightarrow \pi 2p_{3/2}$  transitions. Comparing the results for <sup>44</sup>Ar and <sup>64</sup>Fe, we can conclude that under the influence of the pairing and temperature, the behavior of the low-energy states also

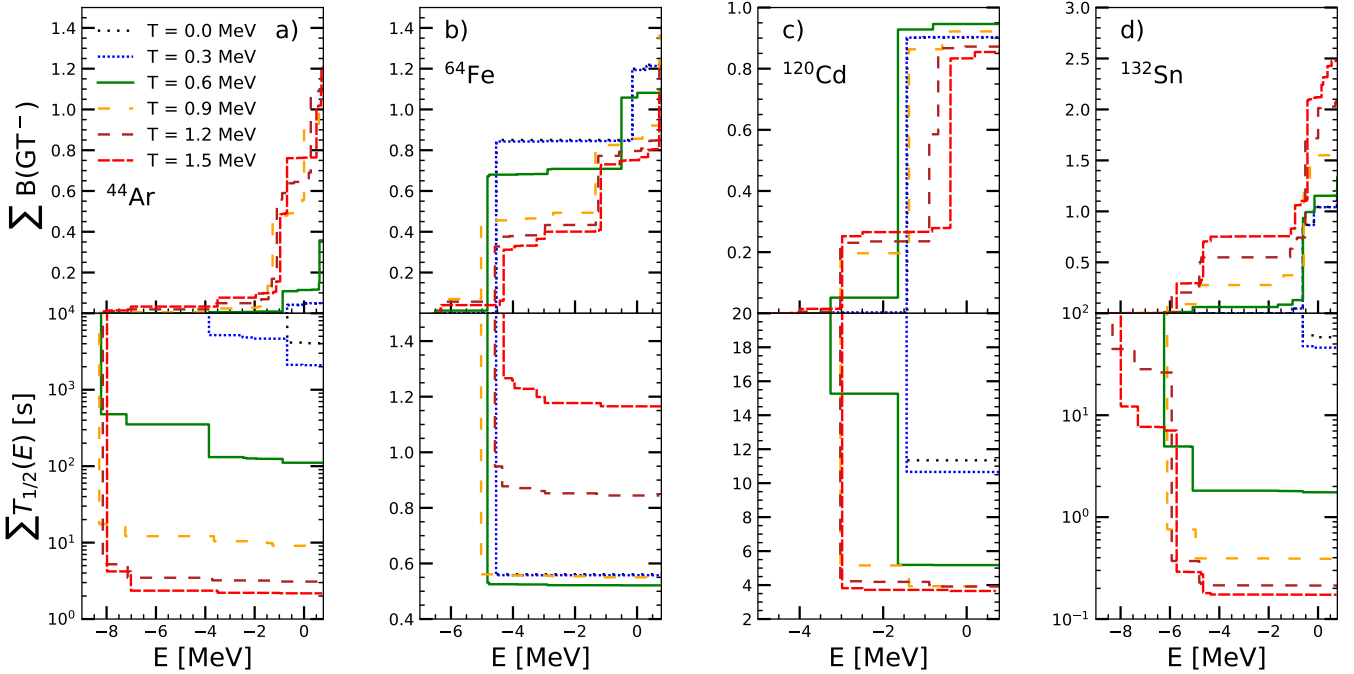


FIG. 4. The cumulative sum of  $GT^-$  strength (upper panel) in the  $Q_\beta$  energy window and of the  $\beta$ -decay half-life  $T_{1/2}$  (lower panel) for temperatures between  $T = 0 - 1.5$  MeV, calculated by considering  $1^+$  multipole transitions for  $^{44}\text{Ar}$ ,  $^{64}\text{Fe}$ ,  $^{120}\text{Cd}$  and  $^{132}\text{Sn}$ .

depends on the particular shell structure and interplay between the pairing and temperature effects, as discussed in Ref. [42].

The evolution of  $GT^-$  strength for  $^{120}\text{Cd}$  with temperature is displayed in Fig. 3(c). At zero temperature, there is only one contribution to the total strength, relevant for  $\beta$ -decay, at  $E = -1.43$  MeV with  $B(GT^-) = 0.90$  due to  $\nu 1g_{7/2} \rightarrow \pi 1g_{9/2}$  transition. Up to  $T = 0.3$  MeV, the  $GT^-$  strength almost does not change. By increasing temperature further, pairing effects start to decrease gradually. At  $T = 0.6$  MeV, the main peak is found at  $E = -1.65$  MeV with  $B(GT^-) = 0.88$ , which is mainly formed with the  $\nu 1g_{7/2} \rightarrow \pi 1g_{9/2}$  transition. Formation of a new excited state with quite low strength is also obtained at  $E = -3.26$  MeV ( $B(GT^-) = 0.05$ ) from the  $\nu 1g_{7/2} \rightarrow \pi 1g_{9/2}$  transition, which in turn increases the phase space and decreases the  $\beta$ -decay half-life. At  $T = 0.9$  MeV, pairing effects vanish completely ( $T_c^{n(p)} \sim 0.7(0.8)$  MeV), and energy of the main peak increases to  $E = -1.38$  MeV while its strength reduces to  $B(GT^-) = 0.67$ . Another peak is found at  $E = -3.02$  MeV with  $B(GT^-) = 0.20$ , which is mainly formed by the same transition  $\nu 1g_{7/2} \rightarrow \pi 1g_{9/2}$ . At  $T = 1.5$  MeV excitation energy of the main peak has further increased to  $E = -0.39$  MeV and its strength reduced to  $B(GT^-) = 0.55$ , while the second peak is found at  $E = -2.98$  MeV and its strength remains almost unchanged. Apart from main  $\nu 1g_{7/2} \rightarrow \pi 1g_{9/2}$  transition, low-energy states start to take contribution from  $\nu 1g_{9/2} \rightarrow \pi 1g_{7/2}$  transition.

From Fig. 4(c) it can be seen that the total  $GT^-$  strength for  $T > 0.6$  MeV decreases, however, the  $\beta$ -decay half-lives continue to decrease slightly due to the formation of new excited states within the  $Q_\beta$  window and increase in the phase space.

Even-even nuclei around  $N = 82$  closed neutron shell are found near the  $r$ -process path, and their  $\beta$ -decay half-lives are especially important for the  $r$ -process nucleosynthesis calculations (see Refs. [1–3]). One such important nucleus is the doubly-magic  $^{132}\text{Sn}$  with a relatively long half-life  $T_{1/2} = 39.7 \pm 0.8$  s [52]. In Fig. 3 (d), we display the  $GT^-$  strength as a function of temperature. Due to the doubly-magic nature of  $^{132}\text{Sn}$ , pairing effects do not play a role in the results and only temperature effect exists. For  $^{132}\text{Sn}$ , new excited states are obtained within the  $Q_\beta$  window due to the unblocking effect of the temperature. The newly formed excited states start to shift downward and their strength also increases with increasing temperature. Therefore, the  $\beta$ -decay phase space increases and the lifetime decreases considerably (see Fig. 2). This can be seen in Fig. 4(d), where newly-formed low-lying strength reduces the half-life by more than an order of magnitude. At  $T = 1.5$  MeV, the state which causes significant reduction of the half-life is found at  $E = -5.73$  MeV, and the most dominant contribution for this state comes from the  $\nu 1h_{9/2} \rightarrow \pi 1h_{11/2}$  transition.

After investigating the effects of temperature in  $\beta$ -decay half-lives, we extend our investigation throughout the nuclide chart. In this work, we focus on nu-

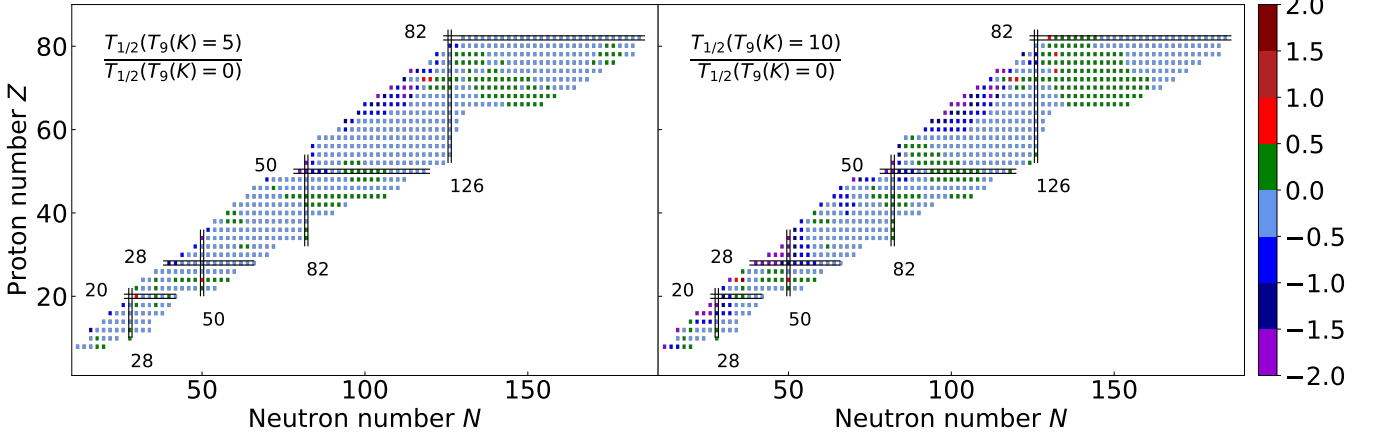


FIG. 5. Ratio between  $\beta$ -decay half-lives  $T_{1/2}$  at  $T_9(K) = 5$ ,  $T_9(K) = 10$  and at zero-temperature shown in the left and right hand side panels, respectively. Nuclei in the range  $8 \leq Z \leq 82$ , with  $T_{1/2} < 10^4$  s are shown. Calculation has been cut at the neutron drip line. Black lines denote proton and neutron magic numbers for guidance.

clei in the  $8 \leq Z \leq 82$  range. Following previous work from Ref. [27], we perform our calculations for nuclei with half-lives below  $10^4$  s at zero-temperature. Pairing gaps for open-shell nuclei are calculated by adjusting monopole pairing constants  $G_{n(p)}$  (see Refs. [42]) to pairing gaps obtained from five-point formula [55]. Half-lives of doubly-magic nuclei are adjusted to the available experimental half-lives by modifying  $g'$  coupling as previously described. The same value of  $g'$  is kept throughout the isotopic chain. Neutron number is increased up to neutron drip-lines [56]. Results for ratios of half-lives at  $T_9(K) = 5$  and  $10$  ( $T_9(K)$  denoting temperature in  $10^9$  K units) and zero-temperature are displayed in Fig. 5. Already at  $T_9(K) = 5$  (left panel of Fig. 5) temperature effects start to contribute. Most affected are regions close to the valley of  $\beta$ -stability and nuclei with long half-lives where temperature leads to an important decrease in the half-lives, similar to the  $^{132}\text{Sn}$ . Also, the nuclei with magic neutron or proton numbers are highly affected since their half-lives are also longer for these nuclei due to the increased stability of magic shells. At  $T_9(K) = 10$  (right panel of Fig. 5) half-lives are significantly altered due to the temperature effects with many nuclei showing changes larger than one order of the magnitude. Again, nuclei showing the most change are those with initially long half-lives (magic, semi-magic, and close to the valley of stability). Also, it can be seen that the effect of the temperature is not universal, namely, while the half-lives can decrease for some nuclei, they can increase for others with increasing temperature. The behavior of the half-lives with increasing temperature depends on the particular shell structure and the pairing properties of nuclei, as discussed above.

In this Letter, we have developed a microscopic framework for the description of temperature dependence of  $\beta$ -decay half-lives, based on the relativistic nuclear energy density functional with the momentum-dependent

meson-nucleon couplings (D3C\* parameterization). The FT-PNRQRPA has been implemented in order to account for allowed and first forbidden transitions relevant for  $\beta$ -decay, by including both the nuclear pairing and finite temperature effects. After benchmarking the model to reproduce the measured half-lives at zero temperature, it was demonstrated that temperature can have a considerable effect on nuclei with longer half-lives, namely, for nuclei with magic numbers and close to the valley of  $\beta$ -stability. By increasing temperature, the excited states start to shift downward and new states appear in the low-energy region due to the unblocking mechanism of the temperature, which in turn leads to an increase in the  $\beta$ -decay phase space, and decrease in the half-lives. The situation becomes more complex for open-shell nuclei and the half-lives can decrease or increase with increasing temperature, depending on the particular shell structure and interplay between the pairing temperature effects of the considered nuclei. It is also shown that the impact of the forbidden-transitions on the half-lives becomes more pronounced with increasing temperature due to the thermal unblocking effect. The presented model is most suitable for large scale calculations of  $\beta$ -decay half-lives at finite-temperature throughout the nuclide chart, relevant for astrophysical nucleosynthesis mechanisms. At an initial study toward this direction, the half-lives are calculated for  $T_9(K) = 5$  and  $T_9(K) = 10$  for nuclei in the range  $8 \leq Z \leq 82$ . Although temperatures where half-lives change significantly appear higher than some of the nucleosynthesis mechanisms (e.g.,  $r$ -process in Ref. [3]), temperature-dependent  $\beta$ -decay half-lives could be important in initial stages of  $r$ -process [57] or astrophysical processes like  $rp$ -process [58] and dense thermonuclear explosions [59] where temperatures are higher. More sophisticated finite-temperature RHB theory, providing accurate scattering of quasiparticle pairs to nuclear continuum, instead of the BCS for ground state-

calculations, is going to be developed and implemented in forthcoming studies. Improved description throughout the nuclide chart by including the half-lives of odd- $A$  nuclei and deformation effects, also necessary for a complete understanding of temperature effects on the  $r$ -process, is going to be addressed in our future studies.

## I. ACKNOWLEDGEMENTS

We thank Tomislav Marketin for helpful discussions. This work is supported by the QuantiXLie Centre of Ex-

cellence, a project co financed by the Croatian Government and European Union through the European Regional Development Fund, the Competitiveness and Cohesion Operational Programme (KK.01.1.1.01). This article is based upon work from the “ChETEC” COST Action (CA16117), supported by COST (European Cooperation in Science and Technology). Y. F. N. acknowledges the support from the Fundamental Research Funds for the Central Universities under Grant No. Lzujbky-2019-11.

- 
- [1] M. Mumpower, J. Cass, G. Passucci, R. Surman, and A. Aprahamian, *AIP Advances* **4**, 041009 (2014).
- [2] K. Langanke and G. Martínez-Pinedo, *Rev. Mod. Phys.* **75**, 819 (2003).
- [3] M. Mumpower, R. Surman, G. McLaughlin, and A. Aprahamian, *Progress in Particle and Nuclear Physics* **86**, 86 (2016).
- [4] I. S. Towner and J. C. Hardy, *Reports on Progress in Physics* **73**, 046301 (2010).
- [5] C. S. Wu, E. Ambler, R. W. Hayward, D. D. Hopps, and R. P. Hudson, *Phys. Rev.* **105**, 1413 (1957).
- [6] H. Liang, N. V. Giai, and J. Meng, *Phys. Rev. C* **79**, 064316 (2009).
- [7] E. Burbidge, G. Burbidge, W. Fowler, and F. Hoyle, *Reviews of Modern Physics* **29**, 547 (1957), cited By 2039.
- [8] J. J. Cowan, F.-K. Thielemann, and J. W. Truran, *Physics Reports* **208**, 267 (1991).
- [9] C. Freiburghaus, S. Rosswog, and F.-K. Thielemann, *The Astrophysical Journal* **525**, L121 (1999).
- [10] B. S. Meyer, G. J. Mathews, W. M. Howard, S. E. Woosley, and R. D. Hoffman, *Astrophys. J.* **399**, 656 (1992).
- [11] G. M. Fuller, W. A. Fowler, and M. J. Newman, *The Astrophysical Journal Supplement Series* **42**, 447 (1980).
- [12] G. M. Fuller, W. A. Fowler, and M. J. Newman, *Astrophysical Journal Supplement Series* **48**, 279 (1982).
- [13] G. M. Fuller, W. Fowler, and M. Newman, *Astrophysical Journal Supplement Series* **252**, 715 (1982).
- [14] G. Fuller, W. Fowler, and M. Newman, *Astrophysical Journal Supplement Series* **293**, 1 (1985).
- [15] T. Oda, M. Hino, K. Muto, M. Takahara, and K. Sato, *Atomic Data and Nuclear Data Tables* **56**, 231 (1994).
- [16] K. Langanke and G. Martínez-Pinedo, *Atomic Data and Nuclear Data Tables* **79**, 1 (2001).
- [17] T. Suzuki, T. Yoshida, T. Kajino, and T. Otsuka, *Phys. Rev. C* **85**, 015802 (2012).
- [18] T. Suzuki, H. Toki, and K. Nomoto, *The Astrophysical Journal* **817**, 163 (2016).
- [19] T. Suzuki, S. Shibagaki, T. Yoshida, T. Kajino, and T. Otsuka, *The Astrophysical Journal* **859**, 133 (2018).
- [20] P. Möller, B. Pfeiffer, and K.-L. Kratz, *Phys. Rev. C* **67**, 055802 (2003).
- [21] M. T. Mustonen and J. Engel, *Phys. Rev. C* **93**, 014304 (2016).
- [22] T. Shafer, J. Engel, C. Fröhlich, G. C. McLaughlin, M. Mumpower, and R. Surman, *Phys. Rev. C* **94**, 055802 (2016).
- [23] Z. Y. Wang, Y. F. Niu, Z. M. Niu, and J. Y. Guo, *Journal of Physics G: Nuclear and Particle Physics* **43**, 045108 (2016).
- [24] J. Engel, M. Bender, J. Dobaczewski, W. Nazarewicz, and R. Surman, *Phys. Rev. C* **60**, 014302 (1999).
- [25] Z. M. Niu, Y. F. Niu, H. Z. Liang, W. H. Long, T. Nikšić, D. Vretenar, and J. Meng, *Physics Letters B* **723**, 172 (2013).
- [26] T. Marketin, D. Vretenar, and P. Ring, *Phys. Rev. C* **75**, 024304 (2007).
- [27] T. Marketin, L. Huther, and G. Martínez-Pinedo, *Phys. Rev. C* **93**, 025805 (2016).
- [28] T. Marketin, E. Litvinova, D. Vretenar, and P. Ring, *Physics Letters B* **706**, 477 (2012).
- [29] Y. F. Niu, G. Colò, M. Brenna, P. F. Bortignon, and J. Meng, *Phys. Rev. C* **85**, 034314 (2012).
- [30] E. Litvinova, B. Brown, D.-L. Fang, T. Marketin, and R. Zegers, *Physics Letters B* **730**, 307 (2014).
- [31] Y. F. Niu, G. Colò, and E. Vigezzi, *Phys. Rev. C* **90**, 054328 (2014).
- [32] Y. F. Niu, Z. M. Niu, G. Colò, and E. Vigezzi, *Phys. Rev. Lett.* **114**, 142501 (2015).
- [33] Y. Niu, Z. Niu, G. Colò, and E. Vigezzi, *Physics Letters B* **780**, 325 (2018).
- [34] E. Litvinova, C. Robin, and H. Wibowo, *Physics Letters B* **800**, 135134 (2020).
- [35] F. Minato and K. Hagino, *Phys. Rev. C* **80**, 065808 (2009).
- [36] S. Typel, *Phys. Rev. C* **71**, 064301 (2005).
- [37] P. Ring, *Progress in Particle and Nuclear Physics* **37**, 193 (1996).
- [38] Y. Gambhir, P. Ring, and A. Thimet, *Annals of Physics* **198**, 132 (1990).
- [39] A. L. Goodman, *Nuclear Physics A* **352**, 30 (1981).
- [40] E. Yüksel, E. Khan, K. Bozkurt, and G. Colò, *Eur. Phys. J. A* **50**, 160 (2014).
- [41] E. Yüksel, G. Colò, E. Khan, Y. F. Niu, and K. Bozkurt, *Phys. Rev. C* **96**, 024303 (2017).
- [42] E. Yüksel, N. Paar, G. Colò, E. Khan, and Y. F. Niu, *Phys. Rev. C* **101**, 044305 (2020).
- [43] E. Yüksel, G. Colò, E. Khan, and Y. F. Niu, *Eur. Phys. J. A* **55**, 230 (2019).
- [44] H. Sommermann, *Annals of Physics* **151**, 163 (1983).
- [45] N. Paar, P. Ring, T. Nikšić, and D. Vretenar, *Phys. Rev. C* **67**, 034312 (2003).

- [46] N. Paar, T. Nikšić, D. Vretenar, and P. Ring, *Phys. Rev. C* **69**, 054303 (2004).
- [47] Y. F. Niu, Z. M. Niu, N. Paar, D. Vretenar, G. H. Wang, J. S. Bai, and J. Meng, *Phys. Rev. C* **88**, 034308 (2013).
- [48] E. Kolbe, K. Langanke, G. Martínez-Pinedo, and P. Vogel, *Journal of Physics G: Nuclear and Particle Physics* **29**, 2569 (2003).
- [49] J. C. Hardy and I. S. Towner, *Phys. Rev. C* **79**, 055502 (2009).
- [50] T. Marketin, N. Paar, T. Nikšić, and D. Vretenar, *Phys. Rev. C* **79**, 054323 (2009).
- [51] H. Behrens and W. Bühring, *Nuclear Physics A* **162**, 111 (1971).
- [52] G. Audi, F. Kondev, M. Wang, B. Pfeiffer, X. Sun, J. Blachot, and M. MacCormick, *Chinese Physics C* **36**, 1157 (2012).
- [53] <https://www.nndc.bnl.gov>.
- [54] C. Robin and E. Litvinova, *Phys. Rev. Lett.* **123**, 202501 (2019).
- [55] M. Bender, K. Rutz, P. G. Reinhard, and J. A. Maruhn, *The European Physical Journal A* **8**, 59 (2000).
- [56] J. Erler, N. Birge, M. Kortelainen, W. Nazarewicz, E. Olsen, A. M. Perhac, and M. Stoitsov, *Nature* , 509 (2012).
- [57] X. D. Xu, B. Sun, Z. M. Niu, Z. Li, Y.-Z. Qian, and J. Meng, *Phys. Rev. C* **87**, 015805 (2013).
- [58] R. Wallace and S. Woosley, *The Astrophysical Journal* **45**, 389 (1981).
- [59] H.-T. Janka, K. Langanke, A. Marek, G. Martínez-Pinedo, and B. Möller, *Physics Reports* **442**, 38 (2007).